International Journal on Advanced Science Engineering Information Technology

Vol.10 (2020) No. 6
ISSN: 2088-5334

Design of THz High-Resistivity Silicon-Based Microstrip Antenna for Breast Cancer Imaging

Herry Tony Andhyka[a,1], Catur Apriono[a,2]

[a] *Department of Electrical Engineering, Faculty of Engineering, Universitas Indonesia, Depok, Indonesia*
E-mail: [1]herry.tony@ui.ac.id; [2]catur@eng.ui.ac.id

***Abstract*— Cancer is the second deadliest disease globally, with approximately 18 million cases and 9.6 million deaths in 2018. There were 2.088 million breast cancer cases and 627 thousand deaths. This cancer is the second most prevalent after lung cancer, resulting in the fifth most cancer deaths worldwide. A critically important technique for the detection of primary-stage tumors or cancer is imaging. Early detection of cancer is necessary to minimize the number of fatalities associated with breast cancer. Several techniques have been applied to breast tissue imaging such as computed tomography scans (CT Scans), transrectal ultrasound (TRUS), magnetic resonance imaging (MRI), positron emission tomography (PET), and single-photon emission computed tomography (SPECT), but these techniques have well-known limitations. THz imaging is also one of the techniques for early detection. THz imaging approaches address key deficiencies in alternative techniques and are typically non-ionizing, non-contact, non-destructive, and have a high spatial resolution. An appropriate detector is a crucial aspect of the development of this promising technique. In this report, a THz silicon-based antenna with a frequency centered at 0.312 THz is proposed for application to breast cancer imaging. A silicon substrate has a high permittivity and is useful for device miniaturization. Inset-fed and array techniques are essential for focusing the beamwidth in the desired direction. The results show that the proposed design can be used to develop a directional antenna with reliable performance. This study will contribute to the development of a THz imaging system for early breast cancer detection.**

***Keywords*— THz; antenna; cancer; breast cancer; imaging; silicon.**

I. INTRODUCTION

Cancer is the second deadliest disease globally, with 18 million cases and approximately 9.6 million deaths in 2018 [1], [2]. With 2.088 million cases, breast cancer is one of the most common types of cancer worldwide. This cancer category is the second most prevalent after lung cancer, with 2.093 million cases and 627 thousand deaths. Breast cancer is currently the fifth most common cause of cancer mortality worldwide [3].

Early cancer detection is critical to effective treatment and intervention to minimize morbidity and mortality. An essential technique for the detection of primary-stage tumor or cancer is imaging. To date, several techniques have been utilized by researchers to image breast cancer. These techniques include computed tomography scans (CT scans), magnetic resonance imaging (MRI), positron emission tomography (PET), single-photon emission computed tomography (SPECT), and transrectal ultrasound (TRUS) [4]. However, each of these techniques has well-known limitations. CT scans expose patients to high radiation levels, causing damage to DNA [5]. TRUS is inhibited by a low resolution and poor contrast [6]. MRI often cannot be used to differentiate between malignant tumors and benign disease, which could lead to false reporting [7]. PET has several limitations, including excessive noise and low spatial resolution. Moreover, it is harmful to patients because of the high radiation levels, as in the case of CT scans [8]. SPECT has a high detection sensitivity but low spatial resolution compared to MRI and CT scans [9].

THz imaging is a potential solution to address the aforementioned imaging techniques' deficiencies by operating in the 0.1–10 THz region of the electromagnetic spectrum [10]. THz radiation has unique properties and characteristics. THz radiation is non-ionizing to human cells [10]. This imaging technique is non-contact and does not have a deleterious effect on cells [11]. It also has a relatively high spatial resolution. Compared to other cancer imaging techniques, not only is THz radiation more secure and safe, but it also yields results of superior quality. Thus, this technique can be used to detect early breast cancer, which should result in reduced mortality. In previous investigations, various techniques such as probe detection, a scanning mechanism, a pulsed terahertz system, reflect emission, and THz mammography in the THz range has been used to diagnose and image breast cancer tissue samples [12]–[16]. In this work, a different approach is presented.

An antenna is one of the main components of a wireless electromagnetic system, such as THz biomedical imaging systems. Several investigators have proposed using antennas for breast cancer imaging using FR-4 and Rogers RT5880 as the dielectric substrate [17]–[19]. The main issue associated with using these materials as substrates is that their efficacy for application in the THz region has not been substantiated. Several studies have been conducted on the use of high-resistivity silicon and gallium arsenide as substrate materials for many applications [20]. However, the implementation of microstrip antennas using high-resistivity silicon has several limitations, such as narrow bandwidth, low efficiency, and poor radiation pattern. Surface and bulk micromachining can be used to address these deficiencies, and high-resistivity silicon material can be used as substrates for many applications.

Previous studies have attempted to image and characterize the dielectric properties of breast cancer tissue [21]–[23]. In these investigations, low-frequency microwaves up to 50 GHz were utilized. The results indicated that the dielectric properties of the tissue were relatively high at that frequency. High dielectric properties imply that a considerable gain antenna is required so that the generated waves can effectively propagate through the tissue. It is more difficult to design an antenna for imaging that operates at these frequencies. However, based on the results, it was shown that the dielectric properties are reduced as the frequency increases. Thus, it is possible to design an antenna for breast cancer imaging that operates in the THz range since it likely requires a low gain.

A THz silicon-based antenna that operates at a resonant frequency of 0.312 THz is presented for breast cancer imaging. We used silicon as a substrate material to replace FR-4 and Rogers RT5880, which have been traditionally used[17]–[19]**.** In this investigation, the inset fed and array techniques were used to focus the beamwidth in the desired direction. One of the objectives is to achieve a higher gain using the proposed design due to a substrate's effect with higher dielectric properties.

II. Material and Method

A frequency of 312 GHz was considered in this work based on the results of a research group in Taiwan in which thin breast tissue was imaged [24]. Moreover, groups in France and Germany also successfully performed breast cancer imaging in the 300 – 500 GHz frequency range. The chosen frequency is in this range [25]. The actual breast cancer tumors' actual size varies from less than 1 cm to sizes more than 5 cm [26]. The breast tissue model used in this work had a size of approximately 1 cm, which is ten times the antenna wavelength. This model consists of three main components, including fat, fibrous tissue, and a tumor. The breast tumor is inside the model and is covered with fibrous tissue and fat. Figure 1 is an illustration of the model.

The proposed size of the human breast tissue model is an assumption. We do not know the actual proportion of each component. When an individual develops cancer, the content of the breast tissue such as water and sodium are consumed by the tumor, causing rapid growth [27]. The increased water content of the tumor also increases the dielectric properties [28]. As such, the actual size and proportion of the tumor and the other tissue are unknown.

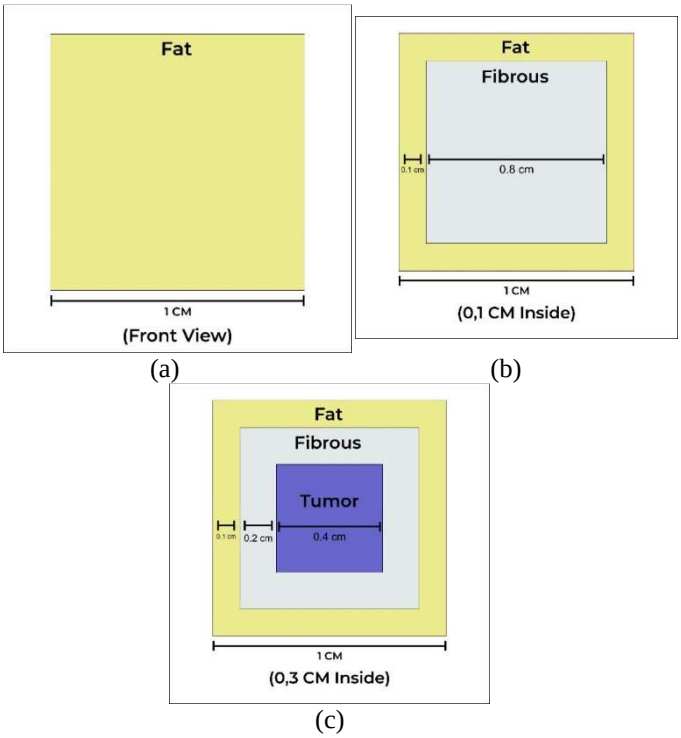

Fig. 1 (a) Front View of the breast tissue model, (b) 0.1 cm inside the breast tissue model, (c) 0.3 cm inside the breast tissue model

Path loss calculations can be used to determine the required gain for the specific antenna design. The losses included in the calculation are the path loss of absorption of both normal tissue and the tumor [29], thermal noise due to the temperature of the body [29], the temperature of the air [30], and also the noise figure. Equation 1 is used to calculate the absorption path losses [29], where α is the coefficient due to absorption, d is the tissue thickness, and e represents the natural or Euler's number. The results for the path loss calculation are shown in Table 1.

$$PL_{abs} = 10\alpha d \, log \, log \, e \quad (1)$$

TABLE I
Absorption Path Loss Calculation

Type	Absorption Coefficient [cm^{-1}]	Thickness [cm]	Absorption Path Loss [dB]
Fat	27.75	0.2	24.103
Fibrous	67.91	0.4	117.971
Tumor	128.27	0.4	222.827
Total		1	364.901

As a result of the occurrence of thermal noise, two path losses must be considered. They include the thermal noise of the body temperature and air temperature. Equation 2 can be used to estimate the noise temperature due to breast tissue absorption prior to calculating the thermal noise of the body temperature [29]. T_{mol} is the equivalent noise temperature due to tissue absorption. T_o represents the reference temperature of 310 K, based on the normal body temperature. For a thickness of 1 cm at a frequency of 312 GHz, the calculated thermal noise associated with breast tissue is 0 K,

which implies that no path loss occurs due to the absorption of breast tissue in the human body. Equation 3 is used to calculate the thermal noise due to air temperature [30], where *k* is the Boltzmann constant, *T* is the temperature of the room, and *B* is the antenna bandwidth. By using an assumed room temperature of 293 K and a 5 GHz bandwidth, the air temperature thermal noise is -106.94 dB. Table 2 shows a summary of the calculation of the thermal noise.

$$T_{mol} = T_0\left(1 - e^{\frac{4\pi f dk}{c}}\right) \quad (2)$$

$$P_N = 10kTB \quad (3)$$

TABLE II
CALCULATED RESULTS FOR THE THERMAL NOISE

Type	temperature [K]	Noise [dB]
Human Body	0	0
Air	293	-106.94
Total		-106.94

Equation 4 is used to calculate the receiver antenna's sensitivity [30], where *NF* is the noise figure. For a total absorption path loss of 364.901 dB, total thermal noise of -106.94 dB, and an assumed noise figure of 1 dB, the receiver antenna's sensitivity is 258.861 dB. Table III shows the results for the total path loss calculation. It can be observed that for THz imaging for breast cancer detection, the loss factor can significantly reduce the radiation power. Therefore, it is necessary to generate high gain radiation, which can be achieved by using a high gain antenna.

$$P_r = PL_{abs} + NF + P_N \quad (4)$$

TABLE III
TOTAL PATH LOSSES

Types	Loss [dB]
Absorption Path Loss	364.901
Thermal Noise	-106.94
Noise Figure	1
Total	258.861

Equation 5 is used to calculate the required gain for both the transmitter antenna and the receiver antenna [30]. λ is the wavelength of the resonant frequency. The symbol of r is the antennas' separation distance, P_T is the power of the transmitter antenna, G_T is the gain of the transmitter antenna, and G_R is the receiver antenna gain. For a wavelength of 962 µm, the separation distance is 1.2 cm, the receiver antenna's sensitivity is 258.861 dB, and assuming a transmitter antenna power of 500 mW, the required gain can be calculated. This calculation is not presented because the value is too large.

$$r = \frac{\lambda}{4\pi}\sqrt{\frac{P_t G_t G_r}{P_r}} \quad (5)$$

Apart from the gain specification, the antenna must satisfy other requirements. For an imaging antenna, the antenna's radiation pattern must be directional with a horizontal and vertical beamwidth directed as close as possible to 0 degrees with 5-degree compensation. Besides, there is no bandwidth standardization for an imaging antenna. Therefore, a bandwidth of 5 GHz is assumed in this work. The antenna design was simulated and optimized using the CST Microwave Studio Software.

III. RESULTS AND DISCUSSION

A. Single Element

Figure 2 shows a top view of the first proposed single element antenna design. This design is a microstrip type antenna considering the use of the high-resistivity silicon with $\mathcal{E}_r$ = 11.9. The patch element is pure copper, which serves as a good conductor. Table IV shows the optimum antenna dimensions after the parameterization process.

TABLE IV
ANTENNA DIMENSIONS

Parameters		Label	Size (µm)
Patch	Length	Lp	155
	Width	Wp	263
	Thickness	Hp	2
Substrate	Length	Ls	500
	Width	Ws	500
	Thickness	Hs	100
Feedline	Width	Wf	38
	Length	Lf	191

Figure 3 shows the return loss result obtained by simulating the antenna design after the parameterization process. The results show that a -48.383 dB return loss is achieved at a frequency centered at 0.312 THz. For a 10 dB boundary, the antenna's bandwidth is approximately 46.59 GHz and ranges from 0.3 GHz to 0.346 GHz. This indicates that the bandwidth requirement is satisfied in the case of the antenna design.

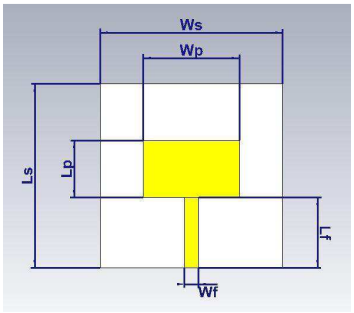

Fig. 2 The top view of single antenna element

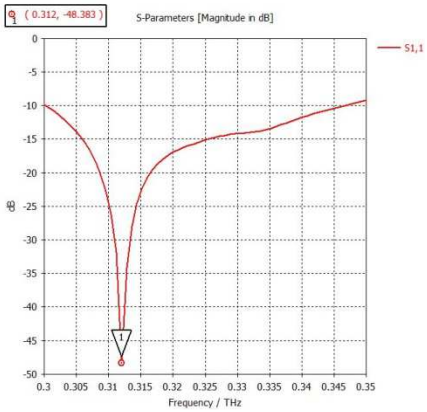

Fig. 3 The return loss of the single-element antenna design antenna

Figures 4-6 show the first antenna design results based on the simulations. These figures show the horizontal and vertical plane radiation patterns, as well as the far-field, respectively. The results indicate that the single element patch antenna is highly directional. This antenna has a horizontal beamwidth of 84 degrees, with the main lobe directed to 0 degrees. This indicates that the horizontal main-lobe specification is met for the proposed antenna design. The antenna also has a vertical beamwidth of 68.7 degrees with the main lobe directed to 17 degrees, which indicates that the vertical main lobe specification is achieved for the antenna design. The simulation results also show that a 4.04 dB gain is achieved. Modifications of the antenna design are needed to meet the antenna specification.

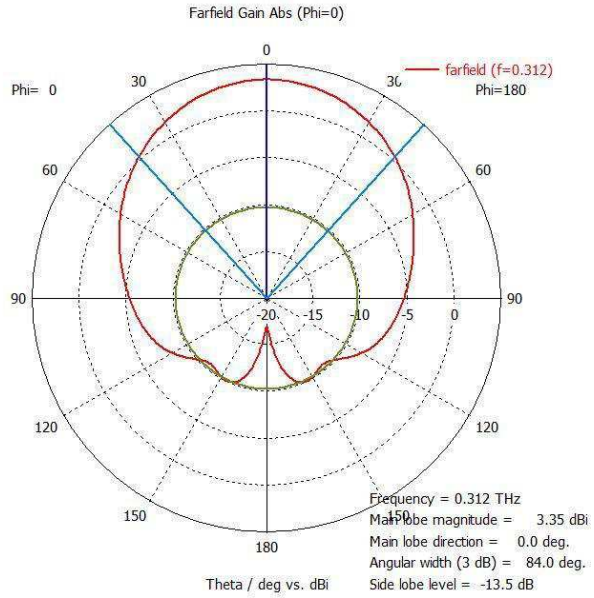

Fig. 4 The horizontal plane pattern of the single antenna element

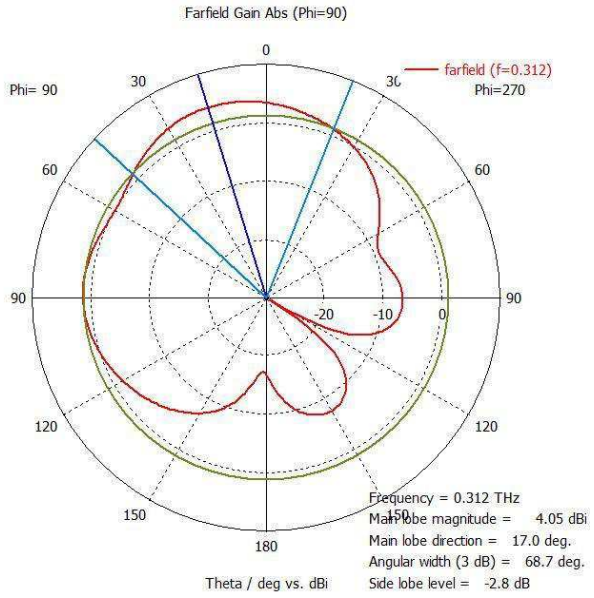

Fig. 5 The vertical plane pattern of the single antenna element

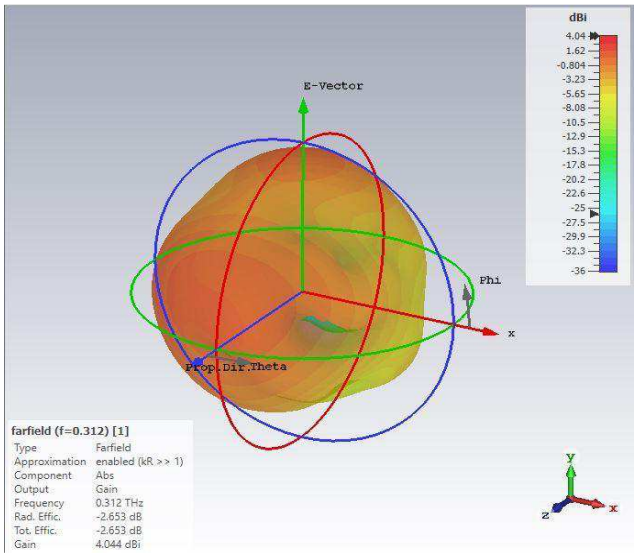

Fig. 6 Far-field result of the single antenna element.

B. *Single Element with Inset-Fed*

Figure 7 shows the top view of a single antenna element based on the inset-fed design. In this case, we add inset fed to the antenna configuration to modify the main lobe direction to satisfy the specification. Table V shows a list of the antenna dimensions after the parameterization process.

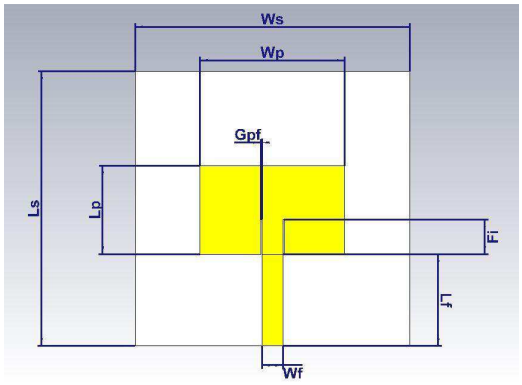

Fig. 7 Top view of the single antenna element with the inset-fed design

Figure 8 shows the return loss based on the simulation results of the antenna after the parameterization process. A -53,445 dB return loss is achieved for a frequency centered at 0.312 THz. For a -10 dB threshold, the antenna's bandwidth is approximately 75.02 GHz and ranges from 0.301 GHz to 0.376 GHz. This indicates that the bandwidth requirement is met for the proposed antenna design.

TABLE V
ANTENNA DIMENSIONS

Parameters		Label	Size (µm)
Patch	Length	Lp	161
	Width	Wp	263
	Thickness	Hp	2
Substrate	Length	Ls	500
	Width	Ws	500
	Thickness	Hs	100
Feedline	Width	Wf	38
	Length	Lf	167
Inset Fed	Width	Gpf	2
	Length	Fi	63

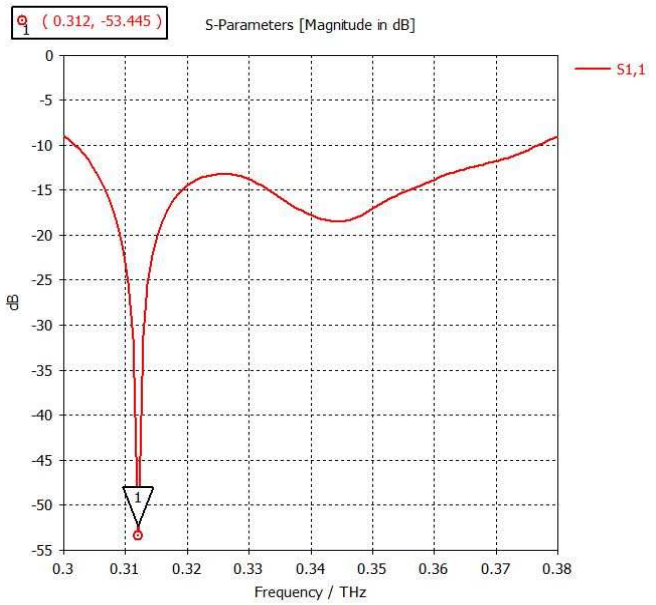

Fig. 8 Return loss result of the single antenna element with the inset-fed design

Figures 9 until 11 show the simulation results for the second antenna design; these figures show the horizontal and vertical plane radiation patterns and the far-field, respectively. The results indicate that the single element patch antenna with an insect-fed design also exhibits high directionality. The antenna has a horizontal beamwidth of 85.5 degrees, with the main lobe directed at 0 degrees. As such, the requirement of the horizontal main lobe is met by the antenna design. The antenna also has a vertical beamwidth of 66.7 degrees, with the main lobe directed at 15 degrees. This indicates that the antenna design meets the specification of the vertical main lobe. The simulation results also show that a 3.27 dB gain is achieved for this antenna. Further modifications of the antenna design are needed to satisfy the antenna specifications.

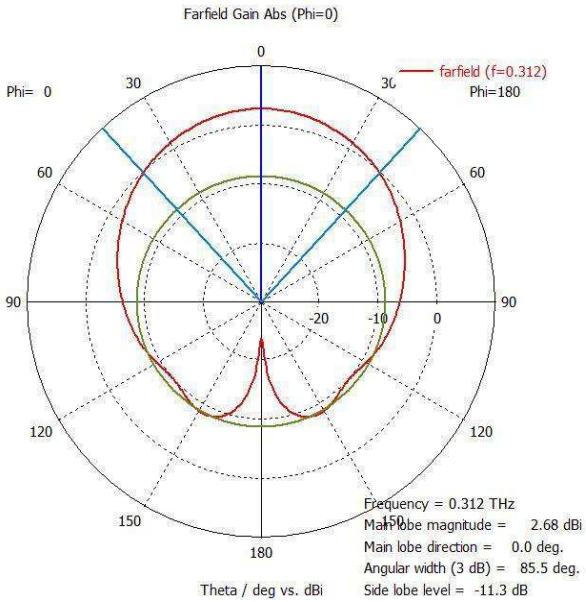

Fig. 9 The horizontal plane pattern of the single antenna element with the inset-fed design

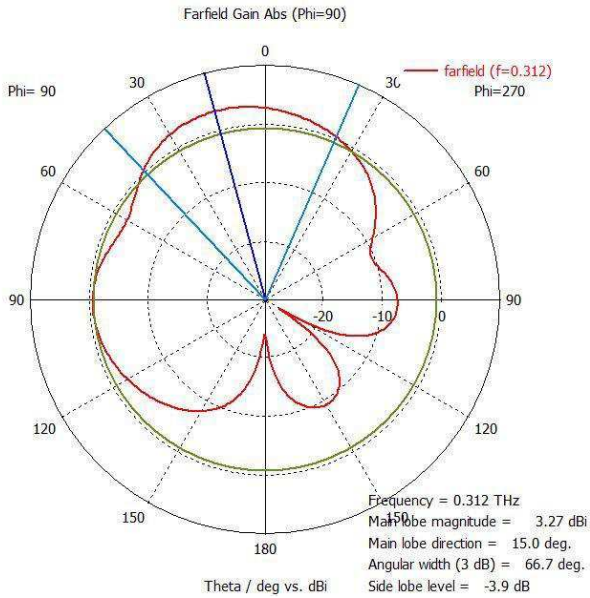

Fig. 10 The vertical plane pattern of the single antenna element with the inset-fed design

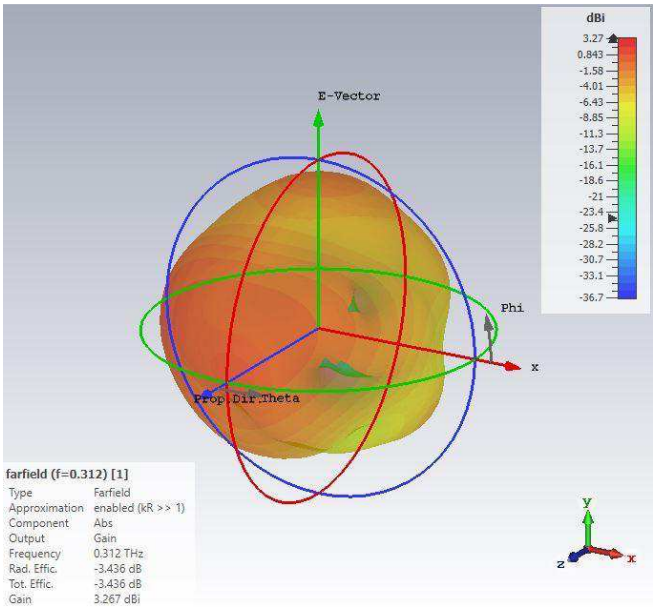

Fig. 11 Far-field result of the single antenna element with the inset-fed design

C. Array Antenna 1X2

In this investigation, we added a vertical element to produce a 1x2 configuration to modify the main lobe direction to achieve the required specification. Figure 12 shows the array antenna design. Table VI is a list of the antenna dimensions after the parameterization process. The second feedline element's length is initially ½ λ or 460 μm, but it changes after the parameterization process.

Figure 13 shows the return loss based on the antenna design's simulation results after the parameterization process. It shows that a -59.203 dB return loss is achieved at a frequency centered at 0.312 THz. For a 10 dB boundary, the antenna's bandwidth is approximately 14.67 GHz and ranges from 0.306 GHz to 0.321 GHz. Thus, the bandwidth requirement is met by the proposed antenna design.

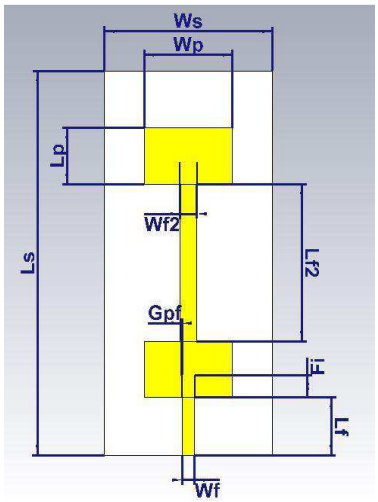

Fig. 12 Top view of the antenna with 1x2 array configuration

TABLE VI
ANTENNA DIMENSIONS

Parameters		Label	Size (µm)
Patch	Length	Lp	161
	Width	Wp	263
	Thickness	Hp	2
Substrate	Length	Ls	1105
	Width	Ws	500
	Thickness	Hs	100
Feedline	Width	Wf	38
	Length	Lf	167
Feedline 2	Width	Wf2	50
	Length	Lf2	452
Inset Fed	Width	Gpf	2
	Length	Fi	63

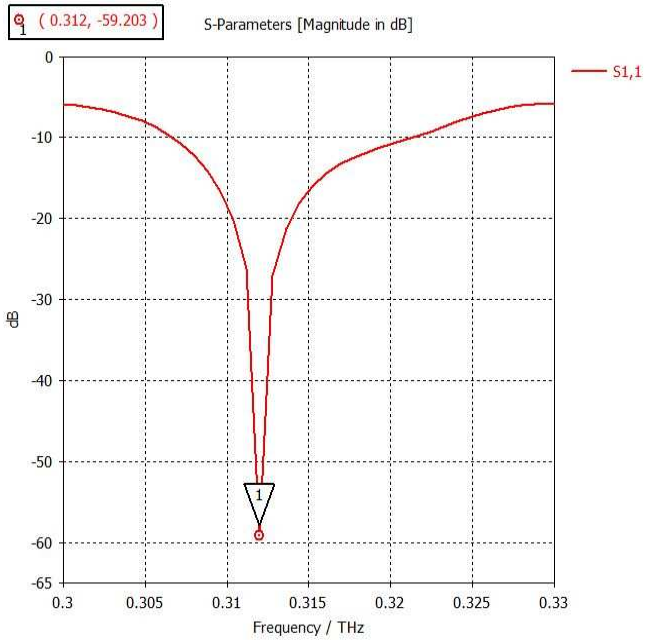

Fig. 13 Return loss result of the antenna with 1x2 array configuration

Figures 14 – 16 show the simulation results of the third antenna design. These results show the horizontal and vertical plane radiation patterns, as well as the far-field, respectively. It is observed that the 1x2 array antenna design is also highly directional. Based on the simulation results, it is determined that the antenna has a horizontal beamwidth of 84.3 degrees with the main lobe directed at 0 degrees. This indicates that the antenna design meets the horizontal main lobe specification. The antenna also has a vertical beamwidth of 39.4 degrees, with the main lobe directed at 3 degrees. This indicates that the antenna design meets the vertical main lobe specification. The simulation results also show that the antenna achieves a 6.04 dB gain. The 1x2 antenna configuration satisfied the overall specifications. Although the antenna met all the specifications, we can still fix the vertical main lobe to 0 degrees for better performance.

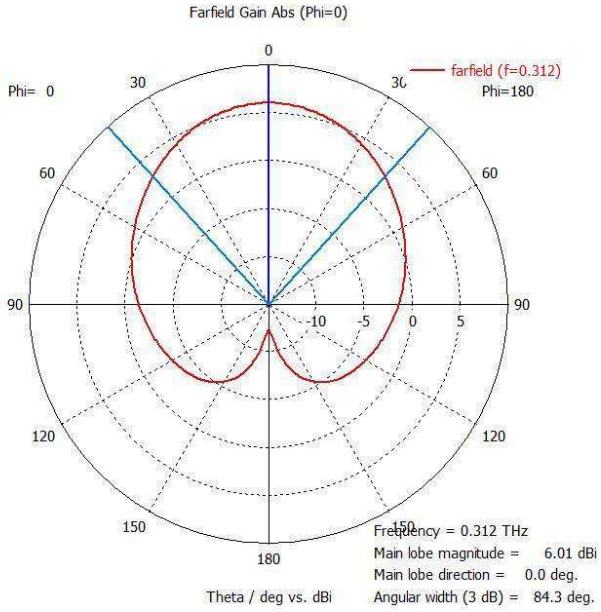

Fig. 14 The horizontal plane pattern of the antenna with 1x2 array configuration

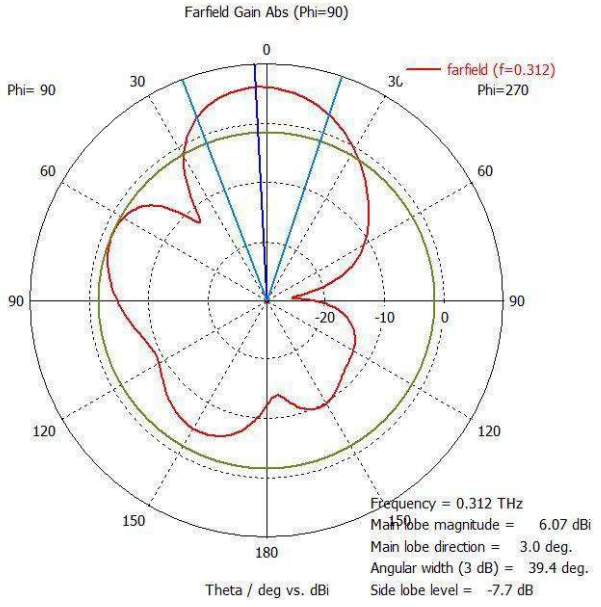

Fig. 15 The vertical plane pattern of the antenna with 1x2 array configuration

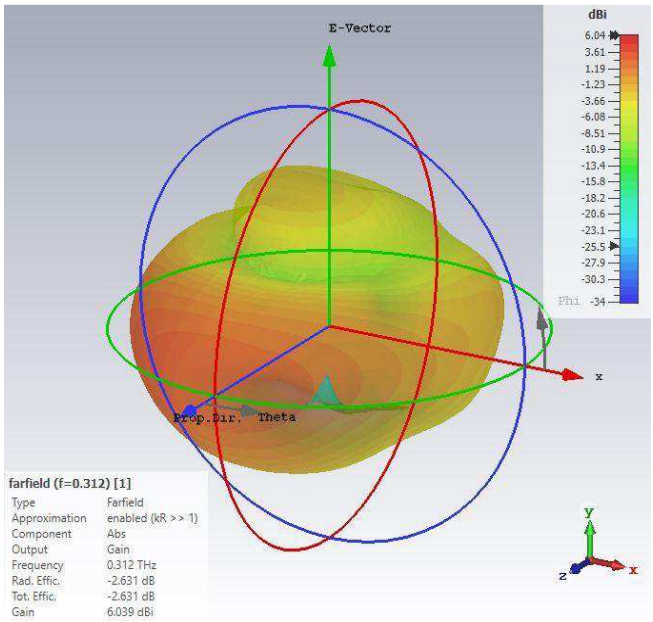

Fig. 16 Far-field result of the antenna with 1x2 array configuration

D. Array Antenna 1X3

In this experiment, we add one more vertical element to produce a 1x3 array configuration to direct the vertical main lobe to 0 degrees to achieve better antenna performance. Figure 17 shows the array antenna design. Table VII shows the list of antenna dimensions after the parameterization process.

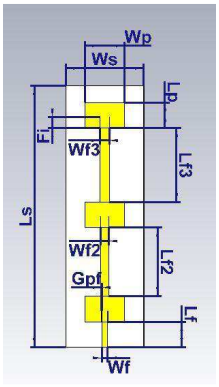

Fig. 17 Top view of the antenna with 1x3 array configuration

TABLE VII
ANTENNA DIMENSION

Parameters		Label	Size (µm)
Patch	Length	Lp	165
	Width	Wp	253
	Thickness	Hp	2
Substrate	Length	Ls	1670
	Width	Ws	500
	Thickness	Hs	100
Feedline	Width	Wf	38
	Length	Lf	161
Feedline 2	Width	Wf2	51
	Length	Lf2	437
Feedline 3	Width	Wf3	57
	Length	Lf3	471
Inset Fed	Width	Gpf	2
	Length	Fi	63

Figure 18 shows the return loss based on the antenna design's simulation results after the parametrization process. It shows that a -40.282 dB return loss is achieved at a frequency centered at 0.312 THz. For a 10 dB boundary, the antenna's bandwidth is approximately 7.09 GHz and ranges from 0.308 GHz to 0.315 GHz. This indicates that the bandwidth requirement is achieved for the antenna design.

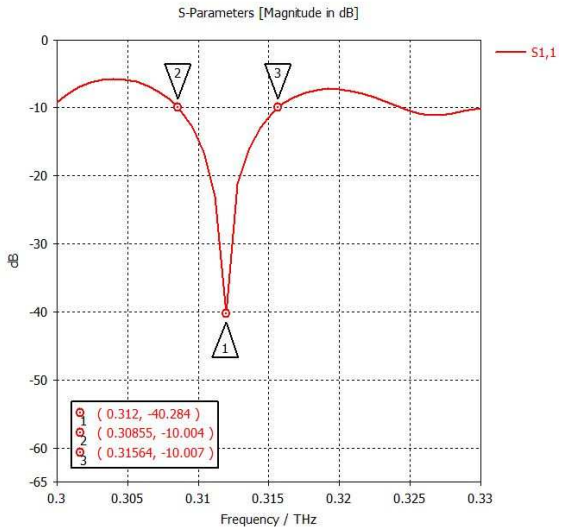

Fig. 18 Return loss result of the antenna with 1x3 array configuration

Figures 19 until 21 show the simulation results of the fourth antenna design. These figures show the horizontal plane and vertical plane radiation pattern, as well as the far-field, respectively. The results show that the 1x3 array antenna design is also highly directional. The antenna has a horizontal beamwidth of 83.9 degrees with the main lobe directed at 0 degrees based on the simulation results. This indicates that the horizontal main lobe specification is achieved for the antenna design. The antenna also has a vertical beamwidth of 29.5 degrees, with the main lobe directed at 0 degrees. This indicates that the vertical main lobe specification is satisfied with the antenna design. The simulation results also show that the antenna achieves a 7.09 dB gain. Overall, the 1x3 array antenna configuration met all the specifications. It can also be observed that the 1x3 array antenna configuration can redirect the vertical main lobe to 0 degrees.

Based on the antenna far-field results, it is evident that the antenna did not achieve its optimum gain. The total efficiency was below 0 dB. This indicates that the substrate traps a component of the total power. An efficiency of 0 dB is considered so that the antenna can achieve superior propagation and gain. It seems that the use of silicon as the substrate material inhibits the effective propagation of the radiation.

Overall, the antenna met most of the requirements. For improved imaging results, the bandwidth must be carefully considered [31]. A small beamwidth was utilized to focus the power to achieve optimal propagation through the tissue. Based on the overall experimental results, the horizontal beamwidth is larger than the vertical beamwidth. The addition of more elements in a horizontal series is one way to minimize the horizontal beamwidth, which can improve the antenna's performance.

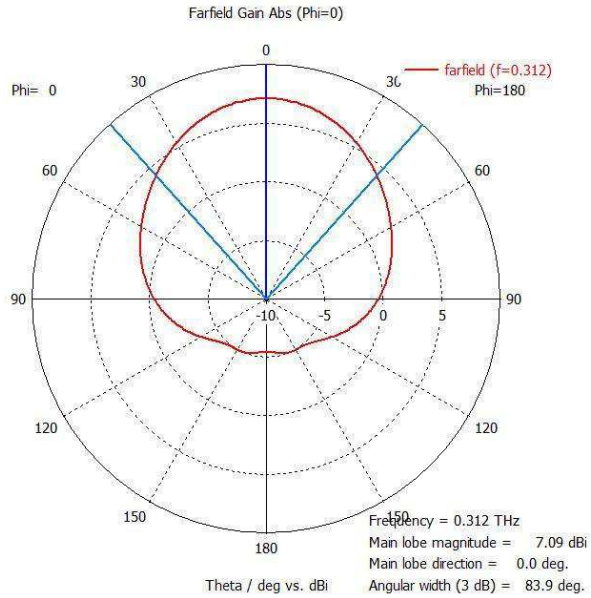

Fig. 19 The horizontal plane pattern of the antenna with 1x3 array configuration

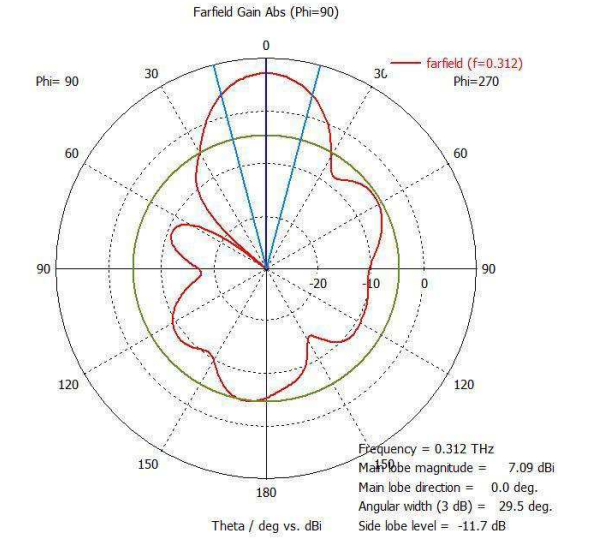

Fig. 20 The vertical plane pattern of the antenna with 1x3 array configuration

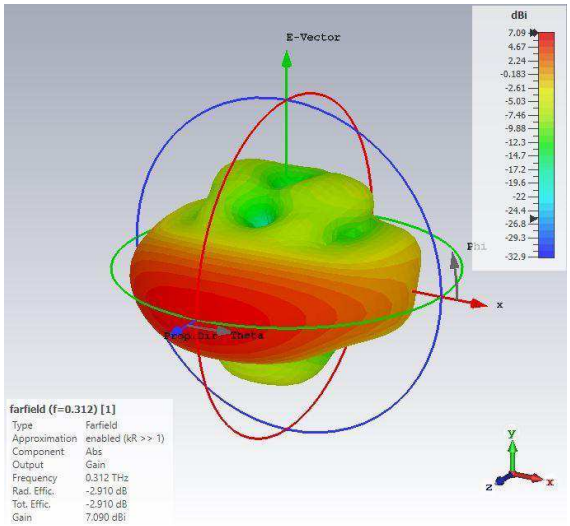

Fig. 21 Far-field result of antenna 1x3 design

IV. Conclusion

The design of rectangular patch array microstrip antennas that were modified with inset fed for breast cancer imaging was reported. Based on the results, the final antenna configuration had a bandwidth of approximately 7 GHz with a frequency centered at 0.312 THz and a gain of 7.09 dB. It had a directional radiation pattern with both horizontal and vertical beamwidth directed at 0 degrees. Based on the simulation results, most of the required specifications were met for the proposed antenna. Only the gain requirement was not met for the proposed antenna. The required gain is very large because the size of the breast model is quite large. One solution is to increase the power input to increase the antenna gain or reduce the breast model's size to reduce the gain requirement.

Acknowledgment

Universitas Indonesia supported this research via the Q1Q2 Grant, the year 2019, contract number: NKB-0292/UN2.R3.1/HKP.05.00/2019.

References

[1] "Cancer." [Online]. Available: https://www.who.int/news-room/fact-sheets/detail/cancer. [Accessed: 04-Apr-2020].

[2] "All Cancers." [Online]. Available: https://gco.iarc.fr/today/data/factsheets/cancers/39-All-cancers-fact-sheet.pdf. [Accessed: 04-Apr-2020].

[3] "Breast." [Online]. Available: https://gco.iarc.fr/today/data/factsheets/cancers/20-Breast-fact-sheet.pdf. [Accessed: 04-Apr-2020].

[4] J. V. Frangioni, "New technologies for human cancer imaging," *J. Clin. Oncol.*, vol. 26, no. 24, pp. 4012–4021, 2008.

[5] H. L. Fred, "Drawbacks and limitations of computed tomography: views from a medical educator," *Texas Hear. Inst. J.*, vol. 31, no. 4, pp. 345–348, 2004.

[6] "MRI CancerQuest." [Online]. Available: https://www.cancerquest.org/patients/detection-and-diagnosis/magnetic-resonance-imaging-mri. [Accessed: 04-Apr-2020].

[7] J. J. Vaquero and P. Kinahan, "Positron Emission Tomography: Current Challenges and Opportunities for Technological Advances in Clinical and Preclinical Imaging Systems," *Annu. Rev. Biomed. Eng.*, vol. 17, no. 1, pp. 385–414, Dec. 2015.

[8] G. L. Gravina et al, "Advances in imaging and in non-surgical salvage treatments after radiorecurrence in prostate cancer: What does the oncologist, radiotherapist and radiologist need to know?" *Eur. Radiol*, vol. 22, no. 12, pp. 2848–2858, 2012.

[9] M. Khalil, J. Tremoleda, T. Bayomy, and W. Gsell, "Molecular SPECT Imaging: An Overview," *Int. J. Mol. Imaging*, vol. 2011, pp. 1–15, 2011.

[10] P. Garbacz, "Terahertz imaging - principles, techniques, and limitations," *Maint. Probl.*, vol. 1–2016, no. April, p. 81, 2016.

[11] J. B. Baxter and G. W. Guglietta, "Terahertz Spectroscopy," *Anal. Chem.*, vol. 83, no. 12, pp. 4342–4368, Jun. 2011.

[12] K. Liu, Q. Sun, X. Chen, A. I. Hernandez-Serrano, and E. Pickwell-Macpherson, "Highly sensitive terahertz imaging method for paraffin embedded cancer samples," *Int. Conf. Infrared, Millimeter, Terahertz Waves, IRMMW-THz*, vol. 2019-Septe, 2019.

[13] H. Chen *et al.*, "High-sensitivity in vivo THz fiber-scanning mammography of early breast cancer in nude mice," *Opt. InfoBase Conf. Pap.*, pp. 5–6, 2011.

[14] A. Portieri, M. Grootendorst, and T. Fitzgerald, "Intra-operative terahertz probe for detection of breast cancer," *2015 8th UK, Eur. China Millim. Waves THz Technol. Work. UCMMT 2015*, pp. 4–5, 2016.

[15] A. Shariffar, T. Bowman, C. Lai, M. Huang, M. El-Shenawee, and K. Bailey, "Modelling the Interaction of THz Waves with Breast Cancer Tissues," *2018 IEEE Antennas Propag. Soc. Int. Symp. Usn. Natl. Radio Sci. Meet. APSURSI 2018 - Proc.*, no. 1, pp. 1843–1844, 2018.

[16] T. Bowman, M. El-Shenawee, and K. Bailey, "Terahertz Imaging of Transgenic Murine Breast Cancer Tumors," *2018 IEEE Antennas Propag. Soc. Int. Symp. Usn. Natl. Radio Sci. Meet. APSURSI 2018 - Proc.*, pp. 901–902, 2018.

[17] I. Nurfitri and C. Apriono, "Radiation Beamwidth Characterization to Enhance Terahertz Imaging Quality for Cancer Detection," in *Proceedings - CAMA 2019: IEEE International Conference on Antenna Measurements and Applications*, 2019, pp. 207–209.

[18] M. V. Hidayat and C. Apriono, "Design of 0.312 THz microstrip linear array antenna for breast cancer imaging application," in *International Conference on Signals and Systems, ICSigSys 2018 - Proceedings, 2018*, 2018, pp. 224–228.

[19] I. Nurfitri and C. Apriono, "Rectangular Linear Array Microstrip Antenna Design for Terahertz Imaging," in *2019 International Conference on Information and Communications Technology (ICOIACT)*, 2019, pp. 719–722.

[20] N. K. Nikolova, M. Ravan, and R. K. Amineh, "Chapter Six - Substrate-Integrated Antennas on Silicon," in *Silicon-Based Millimeter-wave Technology*, vol. 174, M. J. B. T.-A. in I. and E. P. Deen, Ed. Elsevier, 2012, pp. 391–458.

[21] S. Di Meo *et al.*, "Dielectric characterization of material for 3D-printed breast phantoms up to 50 GHz: Preliminary experimental results," *2017 IEEE MTT-S Int. Microw. Work. Ser. Adv. Mater. Process. RF THz Appl. IMWS-AMP 2017*, vol. 2018-Janua, no. September, pp. 1–3, 2018.

[22] Y. Cheng and M. Fu, "Dielectric properties for non-invasive detection of normal, benign, and malignant breast tissues using microwave theories," *Thorac. Cancer*, vol. 9, no. 4, pp. 459–465, 2018.

[23] S. Di Meo *et al.*, "Experimental validation of the dielectric permittivity of breast cancer tissues up to 50 GHz," *2017 IEEE MTT-S Int. Microw. Work. Ser. Adv. Mater. Process. RF THz Appl. IMWS-AMP 2017*, vol. 2018-Janua, no. September, pp. 1–3, 2018.

[24] Son JH, editor. Terahertz biomedical science and technology. CRC Press; 2014.

[25] A. Al-Ibadi *et al.*, "THz spectroscopy and imaging for breast cancer detection in the 300-500 GHz range," *Int. Conf. Infrared, Millimeter, Terahertz Waves, IRMMW-THz*, no. Spp 1857, p. 3853, 2017.

[26] H. G. Welch, P. C. Prorok, A. J. O'Malley, and B. S. Kramer, "Breast-cancer tumor size, overdiagnosis, and mammography screening effectiveness," *N. Engl. J. Med.*, vol. 375, no. 15, pp. 1438–1447, 2016.

[27] M. O'Halloran, D. Byrne, R. C. Conceição, E. Jones, and M. Glavin, "Anatomy and Dielectric Properties of the Breast and Breast Cancer," in *An Introduction to Microwave Imaging for Breast Cancer Detection. Biological and Medical Physics, Biomedical Engineering. Springer, Cham.*, 2016.

[28] M. Hussein, F. Awwad, D. Jithin, H. El Hasasna, K. Athamneh, and R. Iratni, "Breast cancer cells exhibits specific dielectric signature in vitro using the open-ended coaxial probe technique from 200 MHz to 13.6 GHz," *Sci. Rep.*, vol. 9, no. 1, pp. 1–8, 2019.

[29] A. A. N. Chopra, K. Yang, Q. H. Abbasi, K. A. Qaraqe, M. Philpott, "THz Time-Domain Spectroscopy of Human Skin Tissue for In-Body Nanonetworks," *IEEE Trans. Terahertz Sci. Technol.*, vol. 6, no. 6, pp. 803–809, 2016.

[30] Keysight Technologies, "Fundamentals of RF and Microwave Noise Figure Measurements."

[31] T. Binder, "1.6.3 Image Resolution | 123sonography." [Online]. Available: https://www.123sonography.com/content/163-image-resolution. [Accessed: 26-Aug-2020].